

Quantum Phases of Transition Metal Dichalcogenide Moiré Systems

Yiqing Zhou,¹ D. N. Sheng,² and Eun-Ah Kim¹

¹Laboratory of Atomic and Solid State Physics, Cornell University, Ithaca, NY 14853, USA

²Department of Physics and Astronomy, California State University, Northridge, CA 91330, USA

Moiré systems provide a rich platform for studies of strong correlation physics. Recent experiments on hetero-bilayer transition metal dichalcogenide (TMD) Moiré systems are exciting in that they manifest a relatively simple model system of an extended Hubbard model on a triangular lattice. Inspired by the prospect of the hetero-TMD Moiré system's potential as a solid-state-based quantum simulator, we explore the extended Hubbard model on the triangular lattice using the density matrix renormalization group (DMRG). Specifically, we explore the two-dimensional phase space of the kinetic energy relative to the interaction strength t/U and the further-range interaction strength V_1/U . We find competition between Fermi fluid, chiral spin liquid, spin density wave, and charge density wave. In particular, our finding of the optimal further-range interaction for the chiral correlation presents a tantalizing possibility.

The triangular lattice Hubbard model has long been of intense interest [1–14], since the geometric frustration and quantum fluctuation can lead to a rich set of possibilities. In particular, previous density matrix renormalization group (DMRG) studies have shown a robust metal-insulator transition (MIT) at half-filling [4]. More recently, the possibility of the chiral spin liquid (CSL) phase preempting the MIT [7, 12] has been predicted. Other possible ordered phases have been proposed [13]. However, the lack of continuous experimental control over the ratio of the interaction strength and the bandwidth, U/t , the key tuning parameter in theoretical studies, has made it challenging to test these predictions.

Following the proposal of [15] that hetero-bilayer transition metal dichalcogenide (TMD) Moiré systems can realize the triangular lattice Hubbard model, recent experiments on hetero-TMD Moiré systems have indeed observed Mott insulating states at half-filling [16, 17]. Furthermore, continuous control over U/t is now accessible [18, 19]. However, as evidenced by the charge order at fractional fillings [20, 21] the TMD systems have further-range interactions due to a low charge density and resulting low screening. Excitingly, these further-range interactions can also be tuned in experiments [18], presenting a two-dimensional space spanned by U/t and V_1/U to explore a plethora of quantum phases. In comparison, computational investigations have so far been restricted to systems with only on-site interactions.

Motivated by the experimental developments, in this work, we explore the extended Hubbard model on a triangular lattice and study the phase space upon tuning the ratio of hopping to on-site interaction t/U and the relative strengths of long-range interactions V_1/U (Fig.1(b)). Using DMRG, we make the first pass over this large phase space and benchmark our results against the standard Hubbard model limit [4, 5, 7, 12]. By studying the effect of further-range interactions, we study competition between charge order, chiral spin liquid, and spin density wave at half-filling. The rest of the paper is organized as follows: We first introduce the extended Hubbard

model under study and identify a rich phase diagram with Fermi fluid (FF), chiral spin liquid (CSL), and spin density wave (SDW) phases in weak long-range interaction region, showing consistency between the extended Hubbard model in small V_1/U limit and the standard Hubbard model. Interestingly, we find that intermediate long-range interaction can enhance the chiral order. Finally, we discuss the charge-ordered states promoted by stronger long-range interactions. We close with a summary of the quantum phases we observe and provide future outlooks.

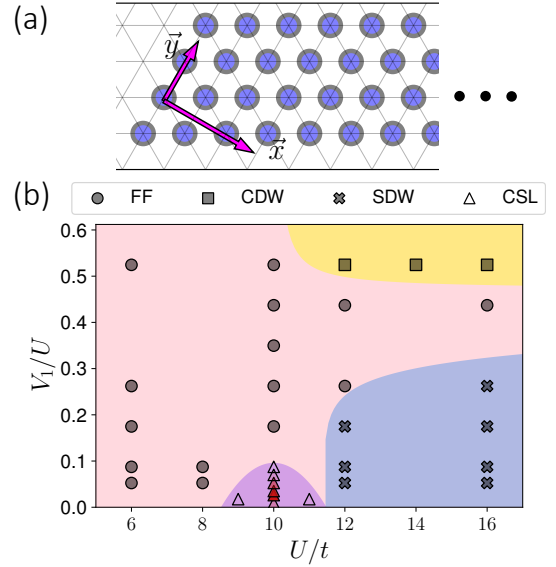


FIG. 1. The system under study and the phase diagram. (a) A partial sketch of a YC4 cylinder used in the DMRG calculation, where x, y directions are specified by the arrows. The number of lattice sites along y direction $L_y = 4$. The boundary condition is periodic in y and open along the cylinder axis direction. (b) The phase diagram of the extended Hubbard model on a triangular lattice. The symbols represent phases observed using DMRG; the color shadings are the schematic extents of the phases. The color intensity of the CSL markers (triangles) represents the strength of chiral ordering.

Model– We consider the following extended Hubbard model on a triangular lattice,

$$H = -t \sum_{\langle ij \rangle} (c_i^\dagger c_j + H.c.) + U \sum_i n_{i,\uparrow} n_{i,\downarrow} + V_1 \sum_{\langle ij \rangle} n_i n_j + V_2 \sum_{\langle\langle ij \rangle\rangle} n_i n_j + V_3 \sum_{\langle\langle\langle ij \rangle\rangle\rangle} n_i n_j, \quad (1)$$

where t, U, V_i represent hopping, on-site interaction, i -th nearest neighbor interaction strength respectively. We choose $V_2/V_1 \approx 0.357$ and $V_3/V_1 \approx 0.260$ to follow an hetero-bilayer TMD experiment setup [18] (derivation shown in Appendix). Given the independent experimental control over the bandwidth and the range of interaction, we explore the ground state in a phase space spanned by the on-site interaction strength, U/t and the further-range interaction strength represented by V_1/U . With the MIT in mind, we focus on the half-filling state at zero total spin $S = 0$. We perform large-scale DMRG calculations on YC4 cylinders as sketched in Fig. 1(a). We compare various cylinder lengths, $L_x = 16, 32, 48$, and keep 10,000 to 28,000 states to get high-accuracy numerical results.

We observe a rich phase space in a parameter space reachable by existing experimental devices. As shown in Fig. 1(b), the phases we observe include chiral spin liquids (CSL), spin density waves (SDW), charge density waves (CDW), and Fermi fluids (FF), with the long-range interactions further enriching the phase space compared to the standard Hubbard model. In the absence of further-range interactions, the system in the large U/t limit can be well-captured by an effective spin model [22] with antiferromagnetic nearest neighbor interaction driven by super exchange on the triangular lattice. The quantum fluctuation in intermediate U/t with the geometric frustration of the triangular lattice might drive CSL[23]. The further-range interaction V_1 can impact the ground state both in the spin and charge sectors. First, in the small V_1/U limit, V_1 interaction enhances the spin exchange interactions by a factor $U/(U - V_1)$, while it can also be mapped to ferromagnetic direct exchange interaction between nearest neighbors, suppressing antiferromagnetic ordering tendencies. This expectation is borne out in our discovery that the chiral order peaks at a finite small V_1/U in the intermediate U/t range as highlighted by the color intensity in Fig. 1(b). Second, as the long-range interaction strength increases, charge order is promoted, and spin ordering is suppressed. Thus we see the melting of CSL and SDW and then the emergence of CDW as V_1/U increases. The richness of the phase space demonstrates the importance of long-range interactions. Beyond the intuitive understanding of these phases, we present detailed numerical evidence for each phase below.

Small V_1/U limit– In the small V_1/U limit ($V_1/U \approx 0.0175$), we reproduce the latest results of the Hubbard model with $V_1/U = 0$ [5, 7, 12]. First, we detect the MIT by calculating the double occupancy, $n_d = \langle n_{\uparrow} n_{\downarrow} \rangle$.

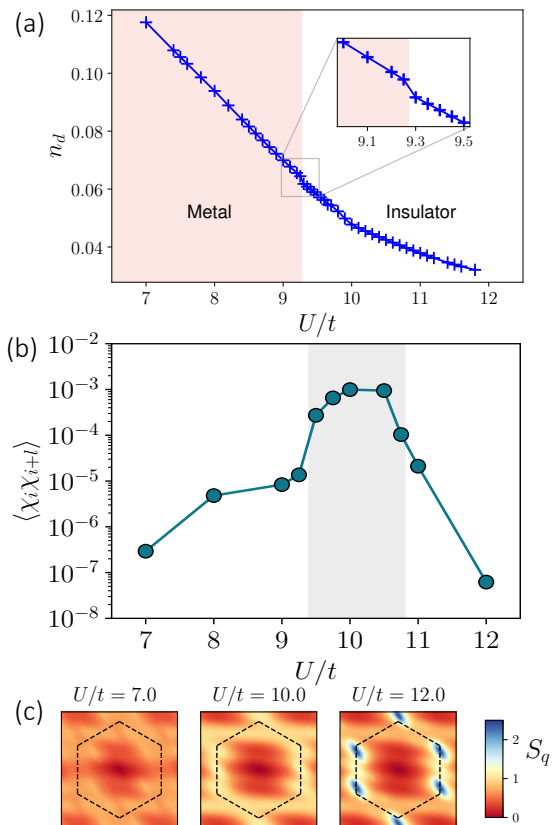


FIG. 2. Small V_1/U limit. (a) Double occupancy n_d as a function of U/t at $V_1/U \approx 0.0175$. The discontinuous drop highlighted in the inset shows the transition from a metallic to an insulating phase. Data is from 4×16 YC cylinder calculations. (b) Chiral correlation function $\langle \chi_i \chi_{i+l} \rangle$ versus U/t at $V_1/U \approx 0.0175$ in a log scale. As a guide to the eye, the grey shaded region marks the range of U/t where CSL lives. (c) Spin structure factors $\langle S_q(\vec{k}) \rangle$ plotted in momentum space at $V_1/U \approx 0.0175$. Three panels correspond to $U/t = 7.0, 10.0$ and 12.0 from left to right, respectively. The black dashed lines mark the boundary of the Brillouin zone. Data is from 4×32 YC cylinders for (b-c).

It shows a discontinuous drop at the critical value of $(U/t)_{\text{MIT}} \sim 9.2$, upon increasing U/t (Fig. 2(a)). This observation is consistent with an earlier study [12], which reports the MIT at $U/t \approx 9.0$ for the Hubbard model. Next, we identify the above metal-insulator transition to take the system into a CSL phase by calculating the spin structure factor (Fig. 2(c)) and the chiral correlation function (Fig. 3). We consider the chiral correlation function $\langle \chi_i \chi_j \rangle$, where the chiral order parameter $\chi_i = \vec{S}_i \cdot (\vec{S}_j \times \vec{S}_k)$ is defined on a triangle centered around lattice site i , involving all three corner sites i, j, k . [24] We observe, in Fig. 2(b) between $U/t \approx 9.4$ and 10.8 , a long-range chiral correlation $\langle \chi_i \chi_j \rangle$ that is orders of magnitude higher than that in neighboring phases. The lower boundary of the long-range chiral correlation $U/t \approx 9.4$ matches where the MIT is observed from the double-occupancy (see Fig. 2(a)). In addition, the featureless spin

structure factor, $\langle S_q(\vec{k}) \rangle = \frac{1}{N} \sum_{ij} e^{i\vec{k}\cdot\vec{r}_{ij}} \langle \vec{S}_i \cdot \vec{S}_j \rangle$ confirms absence of magnetic order associated with the intermediate U/t insulating phase. Note that the slight anisotropy is caused by the finite-size geometry of the YC4 cylinders. Observing long-range chiral correlations that are at the same order of magnitude as reported in Refs. [7, 12] for the Hubbard model with $V = 0$ [25], we conclude that the insulating state immediately after the MIT is CSL.

Increasing U/t further, we observe an additional phase transition within the insulating phase. Upon this second transition, the spin structure factor gains sharp peaks at corners of the Brillouin zone (see Fig. 2(c)). Similar peaks in $\langle S_q(\vec{k}) \rangle$ have been observed in the Hubbard model [5, 12]. These peaks distinguish the large U/t insulating phase from the intermediate U/t CSL phase and evidence the emergence of spin density waves with wave vectors $\mathbf{Q}_{\text{SDW}} = (\sqrt{3}\pi/2a, \pi/2a)$ and $(\sqrt{3}\pi/2a, -\pi/2a)$. At the same time, the chiral correlation dives down, indicating the non-chiral nature of the spin density wave state (see Fig. 2(b)).

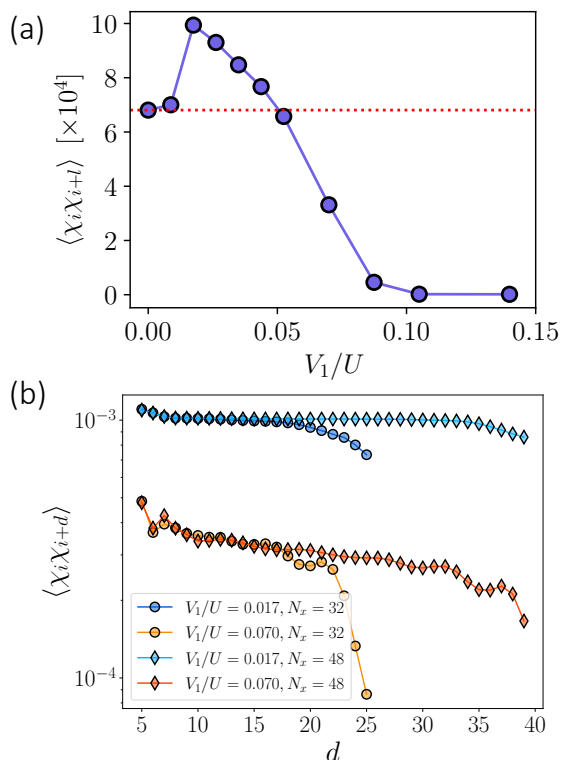


FIG. 3. Chiral correlation function. (a) Chiral correlation function $\langle \chi_i \chi_{i+l} \rangle$ versus V_1/U at $U/t = 10.0$. The red dashed horizontal line denotes $\langle \chi_i \chi_{i+l} \rangle$ at $V_1/U = 0$. Data points are obtained from 4×32 cylinders, and the site separation is chosen to be by half the cylinder length, $l = L_x/2 = 16$. (b) Chiral correlation $\langle \chi_i \chi_{i+d} \rangle$ as a function of site separation d with fixed $U/t = 10.0$ and different V_1/U . Results from two systems sizes, $L_y = 4, L_x = 32$ and 48 are presented.

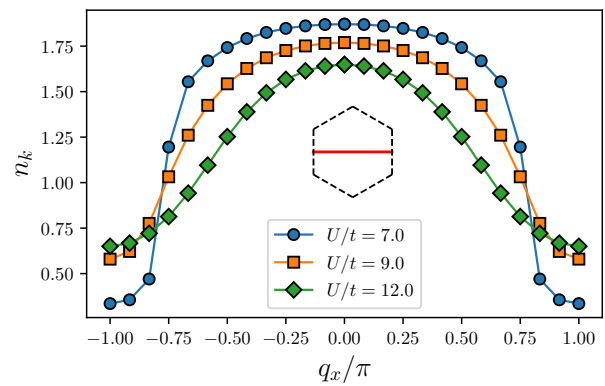


FIG. 4. Electron momentum distribution n_k along a momentum space cut at fixed further-range interaction strength $V_1/U = 0.0175$ and various on-site interaction strengths $U/t = 7.0, 9.0$ and 12.0 . The inset shows a Brillouin zone with the cut marked by the red line.

Effects of further-range interactions – We study phase transitions driven by the further-range interactions, fixing the on-site interaction strength at $U/t = 10$, which is close to the center of the CSL phase. The further-range interaction has a non-monotonic effect on the CSL phase as it is shown through the chiral correlation at half the length of the YC4 cylinder, $l = L_x/2$ as a function of V_1/U in Fig. 3(a). The non-monotonicity comes with the dramatic enhancement in the chiral correlation at intermediate V_1/U compared to the original Hubbard model. Upon further increasing V_1/U , the system leaves the sweet spot, and chiral correlation dies out at $V_1/U \gtrsim 0.07$. Within the CSL phase, we investigate the chiral correlation strength as a function of distance d . As shown in Fig. 3(b), we find the chiral correlation to be long-ranged, nearly constant as a function of d in the CSL phase. We present results from systems with $L_x = 32$ and 48 . Despite the finite-size effects near the end of the cylinder, both systems have consistent chiral correlation strength. The region of nearly constant correlations grows with L_x , indicating true chiral order at large L_x limit.

As V_1/U increases, the CSL melts into a Fermi fluid phase. This FF phase fills in the large space between CSL, SDW, and CDW in the phase diagram. The signature of this phase lies in its electron momentum distribution, $n_k = \frac{1}{N} \sum_{ij} e^{-ikr_{ij}} \langle c_i^\dagger c_j \rangle$. The representative data for FF is obtained at $V_1/U \approx 0.0175$ as shown in Fig. 4. At $U/t = 7.0$, which is in the FF phase, we observe a rapid drop in occupation at $q_x/\pi = 0.75$, resembling a finite residue similar to a Fermi liquid (for larger $U/t \gtrsim 12$ in FF, the nature of the liquid phase becomes more complex and difficult to be characterized, which we leave for future studies). In contrast, other phases show continuous changes in n_k through the Brillouin zone.

In the large U/t region, increasing V_1/U melts the SDW into FF and then drives the formation of CDW. Fig.5(a)

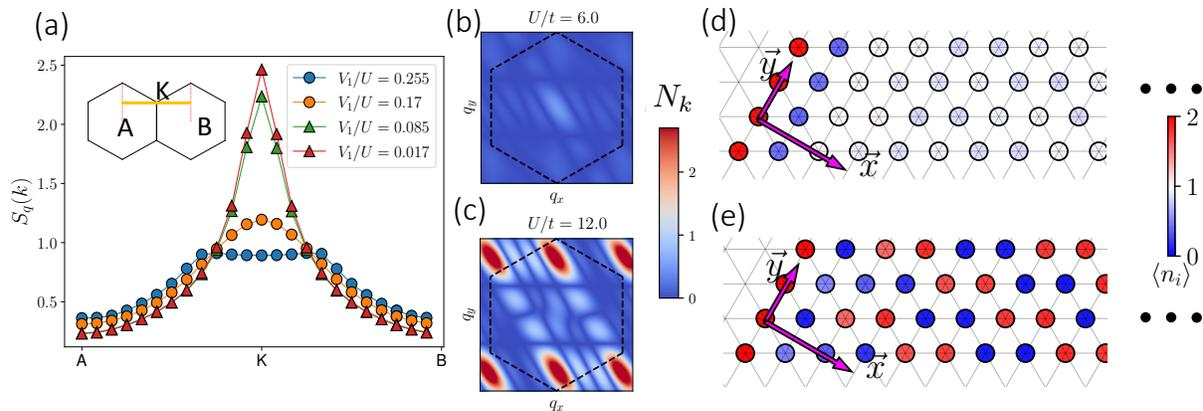


FIG. 5. Large U/t limit. (a) Spin structure factor $S_q(\vec{k})$ with $U/t = 12.0$ at various V_1/U along a cut in momentum space highlighted by the yellow line in the inset. The peaks are observed around the K point. Panels (b)-(e) show charge density at $V_1/U \approx 0.612$. (b) Charge density in momentum space N_k for $U/t = 6.0$. (c) N_k for $U/t = 12.0$. The black dashed lines represent the boundary of the Brillouin zone. (d) Charge density in real space n_i for $U/t = 6.0$. (e) n_i for $U/t = 12.0$.

shows the spin structure factor $\langle S_q(\vec{k}) \rangle$ along a cut in the momentum space. We observe that the amplitude of the $\langle S_q(\vec{k}) \rangle$ peaks decreases as V_1/U increases, and ultimately the peaks disappear at $V_1/U \approx 0.2$. Increasing the further-range interaction strength across $V_1/U \approx 0.2$, we see the FF until the CDW emerges at $V_1/U \approx 0.5$. We identify the existence of CDWs from the charge density with a shift to remove amplitude at zero wave vector, $N_k = \frac{1}{\sqrt{N}} \sum_i (n_i - 1) e^{-ikr}$. As shown in Fig. 5(b), peaks in N_k appear at two corners of the Brillouin zone, corresponding to CDW wavevector $\mathbf{Q}_{\text{CDW}} = (0, \pi/a)$, where a is the lattice constant. Alternatively, in Fig. 5(c), we show the charge density in real space. The charge density modulation in the short direction suggests that the CDWs are interaction-driven rather than an artifact brought by the quasi-1D system geometry.

Conclusion and outlook – In summary, we investigated the triangular lattice Hubbard model with an extended range of interactions, as motivated by recent experimental developments in hetero TMD Moiré systems. Specifically, we explored the two-dimensional phase diagram controlled by the electron hopping t and the further-range interactions V_1 . In the small V_1/U limit, we reproduce results from [5, 7, 12] showing transitions from a metallic state to a chiral spin liquid and then to a spin density wave phase as U/t increases. Upon increasing long-range interactions V_1, V_2 and V_3 , we find that the chiral spin liquid is strengthened with small long-range interaction before it gives way to the metallic state. On the other hand, the spin density wave is continuously weakened by increasing long-range interactions. Further increasing V_1 , the charge density wave emerges with the wavevector that is not dictated by the quasi-1d geometry of the simulation but rather having periodicity in the direction perpendicular to the cylinder long direction (the x direc-

tion as shown in Fig. 5).

The enhancement of chiral correlation with small but finite further-range interaction we observed presents a tantalizing potential. While we cannot rule out the finite size effect, one possible mechanism for such phenomena would be that further-range interaction driven direct exchange can suppress SDW ordering and further frustration. The observation warrants further computational and experimental exploration. In general, the rich phase diagram we uncovered upon tuning the further-range interactions can guide experimental exploration of the new solid-state quantum simulator platform of hetero TMD Moiré systems. It will be natural to extend current work and study finer mesh of the phase space for comparison with future experiments. With an eye towards comparison with experiments, an interesting future direction is to incorporate spin-orbit coupling, which could bring in topological phases as new sets of possibilities.

Acknowledgements: The authors thank Kin Fai Mak and Jie Shan for helpful discussions. Part of the DMRG calculation uses the ITensor package[26]. DMRG simulations at Cornell were carried out on the Red Cloud at the Cornell University Center for Advanced Computing, with the support of the DOE under award DE-SC0018946. EAK and YZ acknowledge support by the National Science Foundation through award #OAC-1934714 (Institutes for Data-Intensive Research in Science and Engineering – Frameworks) and through the NSF MRSEC program (DMR-1719875) for the initial design of the studies. DNS acknowledges the support by the U.S. Department of Energy, Office of Basic Energy Sciences under Grant No. DE-FG02-06ER46305.

-
- [1] P. Sahebsara and D. Sénéchal, Phys. Rev. Lett. **100**, 136402 (2008).
- [2] T. Yoshioka, A. Koga, and N. Kawakami, Phys. Rev. Lett. **103**, 036401 (2009).
- [3] H.-Y. Yang, A. M. Läuchli, F. Mila, and K. P. Schmidt, Phys. Rev. Lett. **105**, 267204 (2010).
- [4] R. V. Mishmash, I. González, R. G. Melko, O. I. Motrunich, and M. P. A. Fisher, Physical Review B **91**, 235140 (2015).
- [5] T. Shirakawa, T. Tohyama, J. Kokalj, S. Sota, and S. Yunoki, Physical Review B **96** (2017), 10.1103/physrevb.96.205130.
- [6] J. Venderley and E.-A. Kim, Phys. Rev. B **100**, 060506 (2019).
- [7] A. Szasz, J. Motruk, M. P. Zaletel, and J. E. Moore, Physical Review X **10**, 021042 (2020).
- [8] Z. Zhu, D. N. Sheng, and A. Vishwanath, “Doped mott insulators in the triangular lattice hubbard model,” (2020), arXiv:2007.11963 [cond-mat.str-el].
- [9] X.-Y. Song, A. Vishwanath, and Y.-H. Zhang, arXiv e-prints (2020), arXiv:2011.10044 [cond-mat.str-el].
- [10] Y. Gannot, Y.-F. Jiang, and S. A. Kivelson, Phys. Rev. B **102**, 115136 (2020).
- [11] A. Szasz and J. Motruk, arXiv e-prints (2021), arXiv:2101.07454 [cond-mat.str-el].
- [12] B.-B. Chen, Z. Chen, S.-S. Gong, D. N. Sheng, W. Li, and A. Weichselbaum, (2021), arXiv:2102.05560 [cond-mat.str-el].
- [13] A. Wietek, R. Rossi, F. Š. I. au2, M. Klett, P. Hansmann, M. Ferrero, E. M. Stoudenmire, T. Schäfer, and A. Georges, (2021), arXiv:2102.12904 [cond-mat.str-el].
- [14] C. Peng, Y.-F. Jiang, Y. Wang, and H.-C. Jiang, “Gapless spin liquid and pair density wave of the hubbard model on three-leg triangular cylinders,” (2021), arXiv:2103.07998 [cond-mat.str-el].
- [15] F. Wu, T. Lovorn, E. Tutuc, and A. H. MacDonald, Physical Review Letters **121**, 026402 (2018).
- [16] E. C. Regan, D. Wang, C. Jin, M. I. B. Utama, B. Gao, X. Wei, S. Zhao, W. Zhao, Z. Zhang, K. Yumigeta, *et al.*, Nature **579**, 359 (2020).
- [17] Y. Tang, L. Li, T. Li, Y. Xu, S. Liu, K. Barmak, K. Watanabe, T. Taniguchi, A. H. MacDonald, J. Shan, *et al.*, Nature **579**, 353 (2020).
- [18] T. Li, S. Jiang, L. Li, Y. Zhang, K. Kang, J. Zhu, K. Watanabe, T. Taniguchi, D. Chowdhury, L. Fu, J. Shan, and K. F. Mak, (2021), arXiv:2103.09779 [cond-mat.str-el].
- [19] A. Ghiotto, E.-M. Shih, G. S. S. G. Pereira, D. A. Rhodes, B. Kim, J. Zang, A. J. Millis, K. Watanabe, T. Taniguchi, J. C. Hone, L. Wang, C. R. Dean, and A. N. Pasupathy, (2021), arXiv:2103.09796 [cond-mat.mes-hall].
- [20] Y. Xu, S. Liu, D. A. Rhodes, K. Watanabe, T. Taniguchi, J. Hone, V. Elser, K. F. Mak, and J. Shan, Nature **587**, 214 (2020).
- [21] C. Jin, Z. Tao, T. Li, Y. Xu, Y. Tang, J. Zhu, S. Liu, K. Watanabe, T. Taniguchi, J. C. Hone, L. Fu, J. Shan, and K. F. Mak, (2020), arXiv:2007.12068 [cond-mat.mes-hall].
- [22] A. H. MacDonald, S. M. Girvin, and D. Yoshioka, Phys. Rev. B **37**, 9753 (1988).
- [23] T. Cookmeyer, J. Motruk, and J. E. Moore, arXiv e-prints (2021), arXiv:2103.07438 [cond-mat.str-el].
- [24] We consider the chiral correlation function instead of the chiral order parameter because we use real wavefunction for the ground state where the $\langle \chi_i \rangle = 0$ due to time-reversal symmetry.
- [25] The chiral order parameter χ in this work is defined in terms of the spin operators, which differs from the definition using Pauli matrices [7] by a factor of 1/8.
- [26] M. Fishman, S. R. White, and E. M. Stoudenmire, “The ITensor software library for tensor network calculations,” (2020), arXiv:2007.14822.

APPENDIX: DERIVATION OF V_2/V_1 AND V_3/V_1

This appendix shows the derivation of the V_2/V_1 and V_3/V_1 ratios used in our calculation. We model the double gating setup used in TMD experiments as a parallel capacitor, as shown in Fig. 6. The long-range inter-site interaction

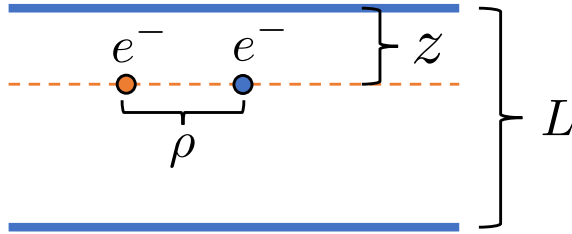


FIG. 6. Parallel capacitor model for TMD placed between double gates. The figure is drawn from a side view, with lines representing planes extending perpendicular to the page. The blue lines represent the top and bottom gates, and the dashed orange line represents the TMD layer. Two electrons in the TMD, represented by the circles, are separated by a distance ρ . The distance between TMD and the top gate is z , and the gate separation is L .

strength is viewed as the potential energy between two electrons separated by distance ρ lying in the TMD layer, which is a plane parallel to the gates. The distance between the plane to the top gate is z , and the gate separation is L . Solving the boundary value problem, we get the potential energy between the two electrons to be

$$V(\rho, z) = \frac{e^2}{\pi\epsilon_0 L} \sum_{n=1}^{\infty} \sin\left(\frac{n\pi z}{L}\right) \sin\left(\frac{n\pi z_0}{L}\right) \mathbf{K}_0\left(\frac{n\pi\rho}{L}\right), \quad (2)$$

where \mathbf{K}_0 is the modified Bessel function. We consider a specific gate-sample geometry with $z = 5$ nm and $L = 35$ nm, and a typical Moiré period of $a_M = 5$ nm. On a triangular lattice, nearest-neighbor interactions have $\rho_1 = a_M$, second nearest neighbors $\rho_2 = \sqrt{3}a_M$ and third nearest neighbors $\rho_3 = 2a_M$. Combining all these data, the model gives $V_2/V_1 \approx 0.357$ and $V_3/V_1 \approx 0.260$.